 CMES, vol.49, no.2, pp.81-110, 2009

An Improved Quadrilateral Flat Element with Drilling Degrees of Freedom for Shell Structural Analysis

H. Nguyen-Van[1] , N. Mai-Duy[1] and T. Tran-Cong[1]

Abstract: This paper reports the development of a simple and efficient 4-node flat shell element with six degrees of freedom per node for the analysis of arbitrary shell structures. The element is developed by incorporating a strain smoothing technique into a flat shell finite element approach. The membrane part is formulated by applying the smoothing operation on a quadrilateral membrane element using Allman-type interpolation functions with drilling DOFs. The plate-bending component is established by a combination of the smoothed curvature and the substitute shear strain fields. As a result, the bending and a part of membrane stiffness matrices are computed on the boundaries of smoothing cells which leads to very accurate solutions, even with distorted meshes, and possible reduction in computational cost. The performance of the proposed element is validated and demonstrated through several numerical benchmark problems. Convergence studies and comparison with other existing solutions in the literature suggest that the present element is efficient, accurate and free of lockings.

Keywords: flat shell, strain smoothing method, shear-locking free, first-order shear deformation theory, drilling degrees of freedom.

1 Introduction

The wide application of shell structures in engineering practice has caught the interests of many researchers in the fields of analysis and design of such structures. A great body of research work has been proposed over several decades towards the development of simple and efficient shell finite elements through three major approaches: (1) the curved shell elements based on classical shell theory with curvilinear coordinates; (2) the degenerated shell elements derived from three-dimensional solid elements and (3) the flat shell elements obtained by the combination of the membrane and bending behaviour of plate elements.

[1] CESRC, Faculty of Engineering & Surveying, USQ, Australia.

In general, it is difficult to identify which shell element is the most advantageous. Among these approaches, the flat shell elements are regarded to be the most attractive as they can be readily built by combining existing plate and membrane elements. They have been used extensively because of the simplicity in their formulation, the effectiveness in performing computation and the flexibility in applications to both shell and folded plate structures. In addition, the performance of the flat shell elements for thick to thin structures also significantly improved with the aid of Reissner-Mindlin kinematics, the incorporation of drilling degrees of freedom (Iura and Atluri, 1992) and the variational principles governing rotations (Atluri, 1980; Atluri and Cazzani, 1994; Atluri, 1984; Suetake, Iura, and Atluri, 2003).

Although triangular flat elements are most efficient for discretizing arbitrary shell geometries, quadrilateral elements are usually used owing to their better performance with respect to convergence rates than that of triangular elements (Lee and Bathe, 2004). The difficulty in the development of the four-node shell element is that such elements are too stiff and suffer from locking phenomenon. This phenomenon originates from the shortcoming in the interpolation of the displacement. Two well-known locking types that may occur in four-node flat elements in analysis of shell structures are (1) the transverse shears locking which arises as the ratio of the thickness-to-characteristic length of a shell becomes small (e.g. $t/L \leq 1/100$), and (2) the membrane locking which occurs when coarse or distorted meshes are used, especially in bending dominated problems.

With the development of shell elements, many methods have been proposed to circumvent these disadvantages. For a summary, the readers are referred to Yang, Saigal, Masud, and Kapania (2000). Techniques to handle shear-locking commonly adopted are the reduced/selective integration (Hughes, Cohen, and Haroun, 1978; Zienkiewicz, Taylor, and Too, 1971; Stolarski and Belytschko, 1983). However, it may lead to the possible manifestation of hourglass modes and stabilization matrices are required to remove these spurious modes (Belytschko and Tsay, 1983; Belytschko, Lin, and Tsay, 1984). An alternative scheme for dealing with the shear-locking problem is the hybrid/mixed formulation in which separate interpolations are used for the stresses and displacements (Lee and Pian, 1978; Noor and Peters, 1981). In another approach to alleviate shear locking, the assumed natural strain method (ANS) first proposed in (MacNeal, 1978, 1982), is generally reported to be an efficient method utilizing complete numerical integration rules. In this approach, the transverse shear strains are interpolated from the displacement-dependent strains defined at the mid-side of element edges to reduce transverse shear locking. Based on this concept, some efficient models were presented, including the mixed interpolated tensorial component (MITC) family proposed by Bathe's group (Dvorkin and Bathe, 1984; Bathe and Dvorkin, 1985) and the discrete strain

gap (DSG) elements proposed by Bischoff's group (Bischoff and Bletzinger, 2001; Koschnick, Bischoff, Camprubi, and Bletzinger, 2005). Another interesting scheme arising from mixed variational formulations is the enhanced assumed strain (EAS) method first presented by Simo and Rifai (1990) and further developed in the linear elastic range (Andelfinger and Ramm, 1993; Cardoso, Yoon, and Valente, 2006) and nonlinear aspects (Bischoff and Ramm, 1997; Eckstein and Basar, 2000; Cardoso, Yoon, and Valente, 2007). The key point of this method lies in the use of a strain field composed of a compatible strain field and an enhanced strain field based on the Hu-Washizu variational principle to reduce shear locking.

Some of these approaches mentioned above are also used to remedy membrane locking, especially the selective reduced integration (SRI) technique and the EAS method. However some of them deteriorate significantly when mesh is distorted (Cardoso, Yoon, and Valente, 2006). More works on the problems related to the membrane locking of flat shell elements can be found in the references of Cook (1994), Groenwold and Slander (1995), Choi and Lee (2003) and Cui, Liu, Li, Zhao, Nguyen, and Sun (2008).

A large number of four-node shell element formulations have been presented to date, showing good performance, however, there is still room to improve the behaviour of flat shell elements, in order to enhance the efficiency, accuracy and stability even when meshes are coarse or elements are badly-shaped. The objective of this study is to propose an improved formulation of a locking-free quadrilateral flat shell element with six degrees of freedom per node that is able to reduce the mesh distortion sensitivity and enhance the coarse mesh accuracy. The present flat element is obtained by applying the strain smoothing method (SSM) to a quadrilateral flat shell element with the combined characteristics of a membrane Allman-type element with drilling DOFs and the assumed strain plate-bending element of Bathe and Dvorkin (1985). The SSM was originally proposed by Chen, Wu, and You (2001) as a normalization for nodal integration of mesh-free Galerkin weak form. Based on this concept, Liu, Dai, and Nguyen (2007) first presented the application of the SSM to the 2D elasticity finite element method as a new smoothed finite element method (SFEM). Further application of SSM for laminated composite plates/shells and piezoelectric solids was presented by Nguyen-Van, Mai-Duy, and Tran-Cong (2007, 2008a,b).

In this study, the membrane part of the proposed shell element is enhanced by applying the SSM instead of the use of hierarchical bubble interpolation mode. The SSM is also applied to the curvature of the plate-bending part to improve the flexural behaviour in the distorted as well as coarse meshes in particular. With the aids of the SSM, the evaluation of bending and membrane stiffness matrices are carried out by integration along the boundary of smoothing elements which can give

more accurate numerical integration even with badly-shaped elements or coarse meshes and also reduce computational time when compared with the evaluation of domain integration. Moreover, the incorporation of the SSM also facilitates relatively simple implementation procedure which makes coding much easier.

In the following sections, a brief review of the four-node flat shell finite element with drilling DOFs is first introduced. This is followed by the strain smoothing approach for the flat shell element. Numerical benchmarks are then conducted to investigate and assess the performance of the proposed 4-node flat shell element before drawing the final conclusions.

2 Finite element formulations of the 4-node flat shell element with drilling degrees of freedom

2.1 Membrane part

The 4-node membrane element with drilling DOFs (Figure 1) is derived by combining the in-plane displacements using Allman-type interpolation functions (Allman, 1984) and the standard bilinear independent normal (drilling) rotation fields. Details of the formulation can be found in the original reference (Ibrahimbegovic, Taylor, and Wilson, 1990) and only a brief review is presented here.

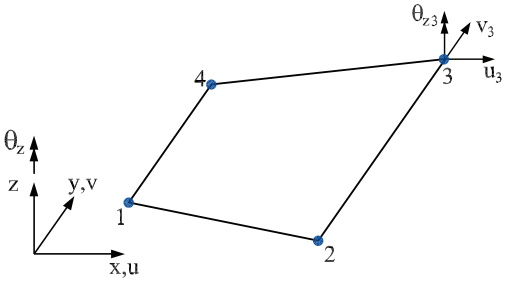

Figure 1: A 4-node quadrilateral element with drilling degrees of freedom

The independent rotation field is interpolated as follows.

$$\theta_z = \sum_{i=1}^{4} N_i(\xi,\eta)\theta_{zi}, \tag{1}$$

and the in-plane displacement fields are approximated by the Allman-type interpolation

$$\mathbf{u} = \begin{bmatrix} u \\ v \end{bmatrix} = \sum_{i=1}^{4} N_i(\xi,\eta) \begin{bmatrix} u_i \\ v_i \end{bmatrix} + \frac{1}{8}\sum_{k=5}^{8} N_k(\xi,\eta)(\theta_{zj}-\theta_{zi}) \begin{bmatrix} y_{ij} \\ x_{ij} \end{bmatrix}, \tag{2}$$

where

$$x_{ij} = x_j - x_i, \qquad y_{ij} = y_j - y_i, \tag{3}$$

$$N_i(\xi,\eta) = \tfrac{1}{4}(1+\xi_i\xi)(1+\eta_i\eta) \qquad i = 1,2,3,4 \tag{4}$$

$$N_k(\xi,\eta) = \tfrac{1}{2}(1-\xi^2)(1+\eta_k\eta) \qquad k = 5,7 \tag{5}$$

$$N_k(\xi,\eta) = \tfrac{1}{2}(1+\xi_k\xi)(1-\eta^2) \qquad k = 6,8. \tag{6}$$

and the ordered triplets (k,i,j) are given by $(5,1,2),\ (6,2,3),\ (7,3,4),\ (8,4,1)$
The linear strain matrix is given by

$$\boldsymbol{\varepsilon}_m = \text{symm}\nabla\mathbf{u} = \sum_{i=1}^{4} \mathbf{B}_{mi}\mathbf{u}_i, \tag{7}$$

where $\mathbf{u}_i = [u_i \quad v_i \quad \theta_{zi}]^T$ is the nodal vector and the gradient matrix $\mathbf{B}_{mi}$ has the following form

$$\mathbf{B}_{mi} = \begin{bmatrix} N_{i,x} & 0 & Nx_{i,x} \\ 0 & N_{i,y} & Ny_{i,y} \\ N_{i,y} & N_{i,x} & Nx_{i,y} + Ny_{i,x} \end{bmatrix}. \tag{8}$$

in which $Nx,\ Ny$ are Allman's incompatible shape functions defined as

$$Nx_i = \frac{1}{8}(y_{ij}N_l - y_{ik}N_m), \tag{9}$$

$$Ny_i = \frac{1}{8}(x_{ij}N_l - x_{ik}N_m). \tag{10}$$

The above indices $i,\ j,\ k,\ l,\ m$ can be expressed in a Matlab-like definition as follows.

$$\begin{aligned} i &= 1,2,3,4;\ m = i+4;\ l = m-1+4*floor(1/i); \\ k &= mod(m,4)+1;\ j = l-4. \end{aligned} \tag{11}$$

where $floor(x)$ rounds the elements of x to the nearest integers towards minus infinity and $mod(x,y)$ is the modulus after division of x by y.
Furthermore, the skew-symmetric part of the strain tensor ($\boldsymbol{\varepsilon}_{sk}$) can be expressed as

$$\boldsymbol{\varepsilon}_{sk} = \text{skew}\nabla\mathbf{u} = \sum_{i=1}^{4} \mathbf{b}_i\mathbf{u}_i + \theta_z, \tag{12}$$

where

$$\mathbf{b}_i = \begin{bmatrix} -\frac{1}{2}N_{i,y} \\ \frac{1}{2}N_{i,x} \\ \frac{1}{16}\left(-y_{ij}N_{l,y}+y_{ik}N_{m,y}+x_{ij}N_{l,x}-x_{ik}N_{m,x}\right)-N_i \end{bmatrix}, \tag{13}$$

and the indices $i,\ j,\ k,\ l,\ m$ are defined by Equation (11).

The variational formulation suggested by Hughes and Brezzi (1989) is described as

$$\Pi_\gamma(\mathbf{u},\theta_z) = \frac{1}{2}\int_\Omega \boldsymbol{\varepsilon}_m^T \mathbf{D}_m \boldsymbol{\varepsilon}_m d\Omega + \frac{1}{2}\gamma\int_\Omega (\boldsymbol{\varepsilon}_{sk}-\theta_z)^2 d\Omega - \int_\Omega \mathbf{u}^T \mathbf{f} d\Omega. \tag{14}$$

Minimization of Equation (14) results in the element membrane stiffness matrix $\mathbf{K}_{mem}$, which is the sum of matrix $\mathbf{K}_m$ and a penalty matrix $\mathbf{P}_\gamma$ as follows.

$$\mathbf{K}_{mem} = \mathbf{K}_m + \mathbf{P}_\gamma = \int_\Omega \mathbf{B}_m^T \mathbf{D}_m \mathbf{B}_m d\Omega + \gamma\int_\Omega \mathbf{b}^T \mathbf{b} d\Omega. \tag{15}$$

The positive penalty parameter γ in Equation (15) is problem dependent. However, the formulation is reported to be insensitive to the value of γ which is taken as the shear modulus value ($\gamma = G$) (Hughes, Brezzi, Masud, and Harari, 1989; Ibrahimbegovic, Taylor, and Wilson, 1990). Many recent numerical studies showed that the smaller value of γ (i.e. value of γ/G between 1/10000 and 1) appeared to give more accurate solutions (Long, Geyer, and Groenwold, 2006; Liu, Riggs, and Tessler, 2000; Pimpinelli, 2004). In this study, $\gamma/G = 1/1000$ is used.

2.2 Plate-bending part

For the plate bending component of the flat shell element, the Mindlin-Reissner type 4-node plate element is employed (Figure 2).

The displacement field $\mathbf{u}$ is approximated as

$$\mathbf{u} = [w \quad \theta_x \quad \theta_y]^T = \sum_{i=1}^{4} \mathbf{N}_i \mathbf{u}_i, \tag{16}$$

where $\mathbf{N}_i$ is the bilinear shape function as in Equation (4) and $\mathbf{u}_i = [w_i \ \ \theta_{xi} \ \ \theta_{yi}]$ is the nodal displacement vector of the element.

The corresponding approximation of curvature is given by

$$\boldsymbol{\kappa} = \begin{bmatrix} \theta_{x,x} \\ \theta_{y,y} \\ \theta_{x,y}+\theta_{y,x} \end{bmatrix} = \mathbf{B}_b \mathbf{u}, \tag{17}$$

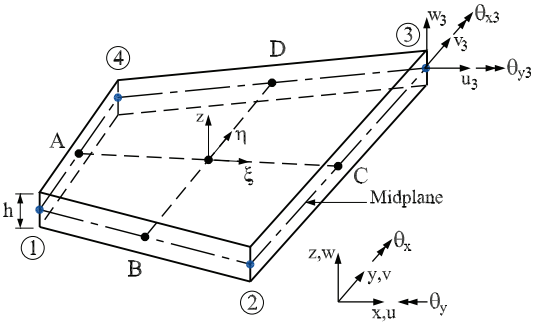

Figure 2: A 4-node quadrilateral plate bending element

where

$$\mathbf{B}_{bi} = \begin{pmatrix} 0 & N_{i,x} & 0 \\ 0 & 0 & N_{i,y} \\ 0 & N_{i,y} & N_{i,x} \end{pmatrix}. \tag{18}$$

The shear strain is approximated with independent interpolation schemes in the natural coordinate system as

$$\begin{bmatrix} \gamma_x \\ \gamma_y \end{bmatrix} = \mathbf{J}^{-1} \begin{bmatrix} \gamma_\xi \\ \gamma_\eta \end{bmatrix} = \mathbf{J}^{-1} \hat{\mathbf{N}} \begin{bmatrix} \gamma_\eta^A \\ \gamma_\xi^B \\ \gamma_\eta^C \\ \gamma_\xi^D \end{bmatrix}, \tag{19}$$

in which

$$\hat{\mathbf{N}} = \frac{1}{2} \begin{bmatrix} (1-\xi) & 0 & (1+\xi) & 0 \\ 0 & (1-\eta) & 0 & (1+\eta) \end{bmatrix}, \tag{20}$$

J is the Jacobian matrix and the midside nodes A, B, C, D are shown in Figure 2. Expressing γ_η^A, γ_η^C and γ_ξ^B,γ_ξ^D in terms of the discretized fields **u**, we obtain the shear matrix

$$\bar{\mathbf{B}}_{si} = \mathbf{J}^{-1} \begin{bmatrix} N_{i,\xi} & b_i^{11} N_{i,\xi} & b_i^{12} N_{i,\xi} \\ N_{i,\eta} & b_i^{21} N_{i,\eta} & b_i^{22} N_{i,\eta} \end{bmatrix}, \tag{21}$$

where

$$b_i^{11} = \xi_i x_{,\xi}^M,\ b_i^{12} = \xi_i y_{,\xi}^M,\ \ b_i^{21} = \eta_i x_{,\eta}^L,\ \ b_i^{22} = \eta_i y_{,\eta}^L, \tag{22}$$

in which $\xi_i \in \{-1,1,1,-1\},\ \eta_i \in \{-1,-1,1,1\}$
and $(i,M,L) \in \{(1,B,A);(2,B,C);(3,D,C);(4,D,A)\}$.

Then through the direct application of variational principles, the element plate-bending stiffness matrix can be obtained as follows.

$$\mathbf{K}_p = \mathbf{K}_b + \mathbf{K}_s = \int_{\Omega^e} \mathbf{B}_b^T \mathbf{D}_b \mathbf{B}_b d\Omega + \int_{\Omega^e} \mathbf{B}_s^T \mathbf{D}_s \mathbf{B}_s d\Omega, \tag{23}$$

where $\mathbf{D}_s,\ \mathbf{D}_b$ are material rigidity matrices for bending and shear, respectively.

2.3 Construction of a flat shell element

The plate bending and membrane formulations presented in the above sections can be combined to form a four-node shell element as shown in Figure 3.

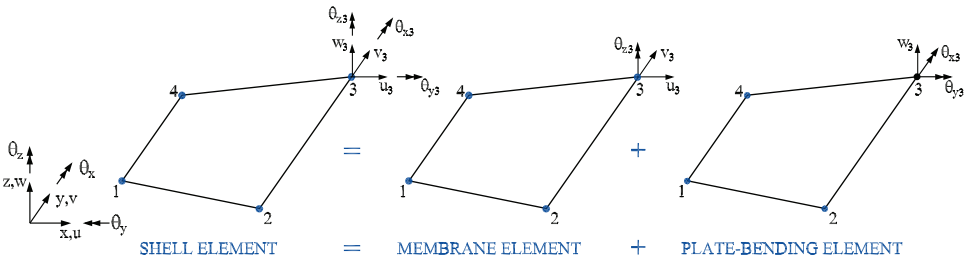

Figure 3: A 4-node quadrilateral flat shell element

When all nodes of the flat shell element are placed in the mid-thickness plane of the shell, the stiffness matrix of a shell element can be formed by combining the plate stiffness and membrane stiffness obtained independently as follows.

$$\mathbf{K}_{flat} = \begin{bmatrix} \mathbf{K}_{mem} & 0 \\ 0 & \mathbf{K}_p \end{bmatrix}. \tag{24}$$

For some shells with double curvature, it may not be possible to have four nodes of the flat shell element on the same plane (warped geometries) and the flat element stiffness must be modified before transformation to the global reference system by using the rigid link correction suggested by Taylor (1987). For the rigid link correction, the mean plane is formed by connecting central points of each side and distances between the mean plane and each nodes are taken to be the same $(|z_i| = h)$. Then, the following displacement transformation equation at each node i

is employed to transform the nodal variables to the projected flat element variables

$$\mathbf{q}'_i = \left\{ \begin{array}{c} u'_i \\ v'_i \\ w'_i \\ \theta'_{xi} \\ \theta'_{yi} \\ \theta'_{zi} \end{array} \right\} = \left[\begin{array}{cccccc} 1 & 0 & 0 & 0 & 0 & 0 \\ 0 & 1 & 0 & 0 & 0 & 0 \\ 0 & 0 & 1 & 0 & 0 & 0 \\ 0 & z_i & 0 & 1 & 0 & 0 \\ -z_i & 0 & 0 & 0 & 1 & 0 \\ 0 & 0 & 0 & 0 & 0 & 1 \end{array} \right] \left\{ \begin{array}{c} u_i \\ v_i \\ w_i \\ \theta_{xi} \\ \theta_{yi} \\ \theta_{zi} \end{array} \right\} = \mathbf{W}_i \mathbf{q}_i, \tag{25}$$

where $\mathbf{W}$ is the projection matrix and z_i defines the warpage offset at each node i perpendicular to the flat mean plane as shown in Figure 4.

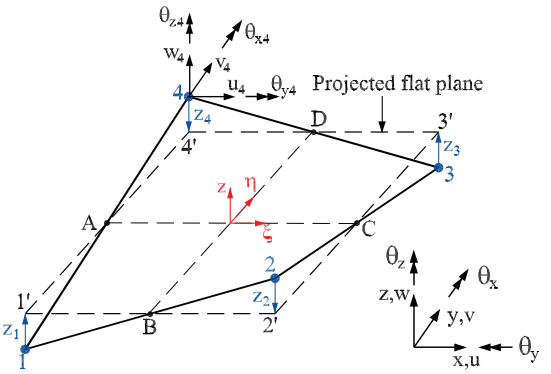

Figure 4: The projection of a warped shell element into a flat mean plane

The local element stiffness matrix, considering the warping effects, is obtained as follows

$$\mathbf{K}_{local} = \mathbf{W}\mathbf{K}_{flat}\mathbf{W}^T. \tag{26}$$

Then the element stiffness in the global reference system $\mathbf{K}_{global}$ is obtained via the rotation matrix $\mathbf{R}$

$$\mathbf{K}_{global} = \mathbf{R}^T\mathbf{K}_{local}\mathbf{R}. \tag{27}$$

3 Strain smoothing approach for flat shell finite element

3.1 Smoothed membrane strain approximation

The membrane strains at an arbitrary point $\mathbf{x}_C$ can be obtained by using the following strain smoothing operation

$$\tilde{\boldsymbol{\varepsilon}}_m(\mathbf{x}_C) = \int_{\Omega_C} \boldsymbol{\varepsilon}_m(\mathbf{x})\Phi(\mathbf{x}-\mathbf{x}_C)d\Omega, \tag{28}$$

where $\boldsymbol{\varepsilon}_m$ is the membrane strain obtained from displacement compatibility condition as given in Equation (7); Ω_C is the smoothing cell domain on which the smoothing operation is performed (Ω_C may be an entire element or part of an element as shown in Figure 5, depending on the stability analysis (Liu, Dai, and Nguyen, 2007)); Φ is a given smoothing function that satisfies at least unity property $\int_{\Omega_C} \Phi d\Omega = 1$ and, in the present work is defined as

$$\Phi(\mathbf{x}-\mathbf{x}_C) = \begin{cases} 1/A_C & \mathbf{x} \in \Omega_C, \\ 0 & \mathbf{x} \notin \Omega_C, \end{cases} \tag{29}$$

in which $A_C = \int_{\Omega_C} d\Omega$ is the area of a smoothing cell (subcell).

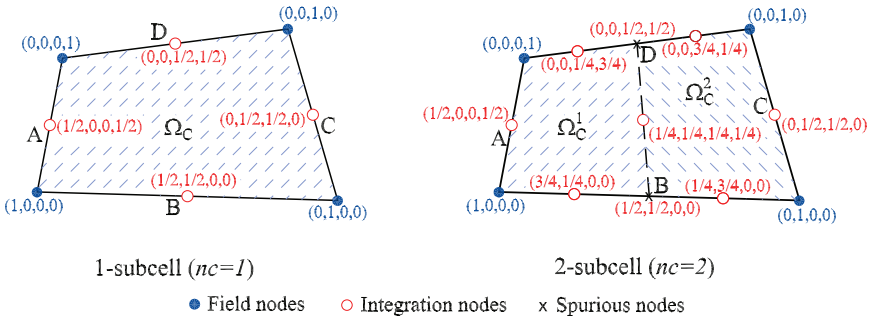

Figure 5: Subdivision of an element into *nc* smoothing cells and values of bilinear shape functions at nodes

Substituting Φ into Equation (28) and applying the divergence theorem, one can get the smoothed membrane strain

$$\tilde{\boldsymbol{\varepsilon}}_m(\mathbf{x}_C) = \frac{1}{2A_C}\int_{\Omega_C}\left(\frac{\partial u_i}{\partial x_j}+\frac{\partial u_j}{\partial x_i}\right)d\Omega = \frac{1}{2A_C}\int_{\Gamma_C}(u_i n_j + u_j n_i)d\Gamma, \tag{30}$$

where Γ_C is the boundary of the smoothing cell.

Introducing the finite element approximation of $\mathbf{u}_m = [u \;\; v \;\; \theta_z]^T$ into Equation (30) gives

$$\tilde{\boldsymbol{\varepsilon}}_m(\mathbf{x}_C) = \tilde{\mathbf{B}}_m(\mathbf{x}_C)\mathbf{u}_m, \tag{31}$$

where

$$\mathbf{u}_{mi} = [u_i \;\; v_i \;\; \theta_{zi}]^T, \tag{32}$$

$$\tilde{\mathbf{B}}_{mi}(\mathbf{x}_C) = \frac{1}{A_C}\int_{\Gamma_C}\begin{pmatrix} N_i n_x & 0 & Nx_i n_x \\ 0 & N_i n_y & Ny_i n_y \\ N_i n_y & N_i n_x & Nx_i n_y + Ny_i n_x \end{pmatrix} d\Gamma. \tag{33}$$

Applying Gauss integration along 4 segments of the boundary Γ_C of the smoothing domain Ω_C, the above equation can be rewritten in algebraic form as

$$\begin{aligned}\tilde{\mathbf{B}}_{mi}(\mathbf{x}_C) = & \frac{1}{A_C}\sum_{b=1}^{4}\begin{pmatrix} \sum_{n=1}^{nG} w_n N_i(\mathbf{x}_{bn}) n_x & 0 & 0 \\ 0 & \sum_{n=1}^{nG} w_n N_i(\mathbf{x}_{bn}) n_y & 0 \\ \sum_{n=1}^{nG} w_n N_i(\mathbf{x}_{bn}) n_y & \sum_{n=1}^{nG} w_n N_i(\mathbf{x}_{bn}) n_x & 0 \end{pmatrix} \\ & + \frac{1}{A_C}\sum_{b=1}^{4}\begin{pmatrix} 0 & 0 & \sum_{n=1}^{nG} w_n Nx_i(\mathbf{x}_{bn}) n_x \\ 0 & 0 & \sum_{n=1}^{nG} w_n Ny_i(\mathbf{x}_{bn}) n_y \\ 0 & 0 & \sum_{n=1}^{nG} w_n Nx_i(\mathbf{x}_{bn}) n_y + \sum_{n=1}^{nG} w_n Ny_i(\mathbf{x}_{bn}) n_x \end{pmatrix}\end{aligned} \tag{34}$$

where nG is the number of Gauss integration points, $\mathbf{x}_{bn}$ the Gauss point and w_n the corresponding weighting coefficients. The first term in Equation (34), which relates to the in-plane translations (approximated by bilinear shape functions), is evaluated by one Gauss point ($nG = 1$). The second term, associated with the in-plane rotations (approximated by quadratic shape functions), is computed using two Gauss points ($nG = 2$).

The smoothed membrane element stiffness matrix can be obtained as

$$\begin{aligned}\tilde{\mathbf{K}}_{mem} = \tilde{\mathbf{K}}_m + \mathbf{P}_\gamma = & \int_\Omega \tilde{\mathbf{B}}_m^T \mathbf{D}_m \tilde{\mathbf{B}}_m d\Omega + \gamma \int_\Omega \mathbf{b}^T \mathbf{b} d\Omega \\ = & \sum_{C=1}^{nc} \tilde{\mathbf{B}}_{mC}^T \mathbf{D}_m \tilde{\mathbf{B}}_{mC} A_C + \gamma \int_\Omega \mathbf{b}^T \mathbf{b} d\Omega\end{aligned} \tag{35}$$

in which *nc* is the number of smoothing cells. To avoid numerically over-stiffening the membrane, one smoothing cell ($nc = 1$) is used in the present formulation. Higher numbers of smoothing cells will lead to stiffer solutions and the accuracy may not be enhanced considerably. The penalty matrix $\mathbf{P}_\gamma$ is integrated using a 1–point Gauss quadrature to suppress a spurious, zero-energy mode associated with the drilling DOFs.

3.2 Smoothed plate-bending strain approximation

In a similar way, by using the same constant smoothing function Φ as for membrane strain, the smoothed curvature matrix can be obtained as

$$\tilde{\boldsymbol{\kappa}}(\mathbf{x}_C) = \int_{\Omega_C} \boldsymbol{\kappa}(\mathbf{x})\Phi(\mathbf{x}-\mathbf{x}_C)d\Omega = \frac{1}{2A_C}\int_{\Gamma_C}(\theta_i n_j + \theta_j n_i)d\Gamma. \tag{36}$$

Then the relationship between the smoothed curvature field and the nodal displacement is written as

$$\tilde{\boldsymbol{\kappa}}(\mathbf{x}_C) = \tilde{\mathbf{B}}_b(\mathbf{x}_C)\mathbf{u}_b, \tag{37}$$

where

$$\mathbf{u}_{bi} = [w_i \;\; \theta_{xi} \;\; \theta_{yi}]^T, \tag{38}$$

$$\tilde{\mathbf{B}}_{bi}(\mathbf{x}_C) = \frac{1}{A_C}\int_{\Gamma_C}\begin{pmatrix} 0 & N_i n_x & 0 \\ 0 & 0 & N_i n_y \\ 0 & N_i n_y & N_i n_x \end{pmatrix} d\Gamma. \tag{39}$$

Using integration with one-point Gauss quadrature to evaluate the above equation over four boundary segment of the smoothing cell we obtain

$$\tilde{\mathbf{B}}_{bi}(\mathbf{x}_C) = \frac{1}{A_C}\sum_{b=1}^{4}\begin{pmatrix} 0 & N_i(\mathbf{x}_b^G)n_x & 0 \\ 0 & 0 & N_i(\mathbf{x}_b^G)n_y \\ 0 & N_i(\mathbf{x}_b^G)n_y & N_i(\mathbf{x}_b^G)n_x \end{pmatrix} l_{bC}. \tag{40}$$

Finally, the plate-bending element stiffness matrix in Equation (23) can be transformed as follows

$$\tilde{\mathbf{K}}_p = \tilde{\mathbf{K}}_b + \mathbf{K}_s = \sum_{C=1}^{nc}\tilde{\mathbf{B}}_b^T\mathbf{D}_b\tilde{\mathbf{B}}_b A_C + \int_{\Omega_e}\mathbf{B}_s^T\mathbf{D}_s\mathbf{B}_s d\Omega. \tag{41}$$

In Equation (41), the shear term $\mathbf{K}_s$ is still computed by 2×2 Gauss quadrature while the element bending stiffness $\tilde{\mathbf{K}}_b$ is computed by one Gaussian point along

each segment of the smoothing cells of the element. In this study, two smoothing cells ($nc = 2$) as shown in Figure 5 are used for calculating the smoothed bending stiffness matrix of the element in order to ensure the rank sufficiency.

The flat shell element stiffness matrix in Equation (24) is then rewritten as

$$\tilde{\mathbf{K}}_{flat} = \begin{bmatrix} \tilde{\mathbf{K}}_{mem} & 0 \\ 0 & \tilde{\mathbf{K}}_{p} \end{bmatrix}. \tag{42}$$

This forms the basis of a new four-node quadrilateral element named MISQ24 (Mixed Interpolation Smoothing Quadrilateral element with 24 DOFs) for analysis of shell structures.

4 Numerical results and discussions

In this section, several benchmark problems are presented to validate and demonstrate the performance of the MISQ24 flat element in shell structural analysis. The developed element performance is compared with that of a fairly complete set of other four-node shell elements in the literature. The list of shell elements used for comparison with the proposed element is outlined in Table 1.

4.1 Scordelis-lo (Barrel vault) roof

The Scordelis-Lo roof provides one of the standard tests to assess the performance of shell elements in a combined bending-membrane problem with the membrane action being dominant. The roof is modelled as a short cylinder shell, loaded by self-weight and supported by rigid diaphragms at the curved edges while the straight edges are free. Geometric, material data and boundary conditions of the problem are shown in the Figure 6.

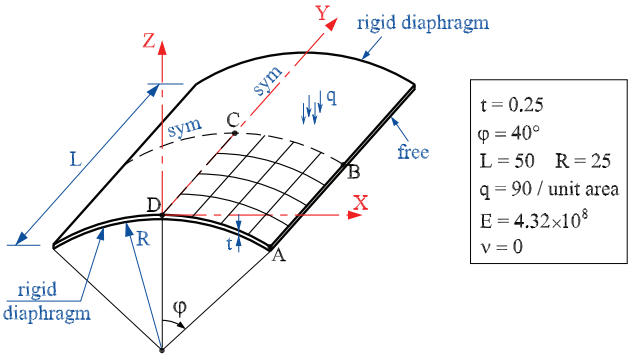

Figure 6: The Scordelis-Lo roof: Geometry and material data

Table 1: List of shell elements used for comparison in the present study.

Name	Brief description
DKQ-4	4-node discrete Kirchoff quadrilateral element of Taylor (1987)
SRI-4	bilinear degenerated shell element, with selective reduced integration of Hughes and Liu (1981)
RSDS-4	bilinear resultant-stress degenerated-shell element, with uniform reduced integration and stability (Liu, Law, Lam, and Belytschko, 1986)
URI-4	4-node uniformly reduced integrated element (Belytschko, Wong, and Stolarski, 1989)
QPH	quadrilateral shell element with physical hourglass control of Belytschko and Leviathan (1994)
IBRA-4	4-node shell element with drilling DOFs developed by Ibrahimbegovic and Frey (1994)
MITC4	4-node fully integrated shell element based on assumed shear strain field of Dvorkin and Bathe (1984)
Mixed	bilinear element with mixed formulation for membrane and bending stress and full 2x2 quadrature of Simo, Fox, and Rifai (1989)
MIN4T	4-node flat shell with drilling DOFs via explicit Kirchhoff constrains (Liu, Riggs, and Tessler, 2000)
NMS-4F	defect-free 4-node flat shell element with drilling DOF (Choi and Lee, 1999)
XSHELL41/42	4-node quasi-conforming flat shell element with driling DOFs (Kim, Lomboy, and Voyiadjis, 2003)
QC5D-SA	4-node flat shell with drilling DOFs and 5-point quadrature by Groenwold and Slander (1995)
SHELL63	4-node thin shell element with drilling DOFs in ANSYS (1998)
T029	4-node Mindlin shell element in Samtech (2003)
Sauer	4-node element proposed by Sauer (1998)
GruWag	4-node element proposed by Gruttmann and Wagner (2005)

According to MacNeal and Harder (1985), the theoretical value for the vertical deflection at the center of the free edge is 0.3086, but a slightly lower value 0.3024 seems to have become the reference solution for many publications. In this study the latter value is used to normalize numerical results. Taking advantage of symmetry, only a quadrant of the roof is discretized and analyzed. Two typical types of mesh, namely $N \times N$ uniform elements and $N \times N$ distorted elements are shown in Figure 7.

Table 2 shows the normalized deflections at the midpoint of the free edge (point B) obtained by the present element with different meshes, together with those of other 4-node shell elements available in the literature. The results show that the present

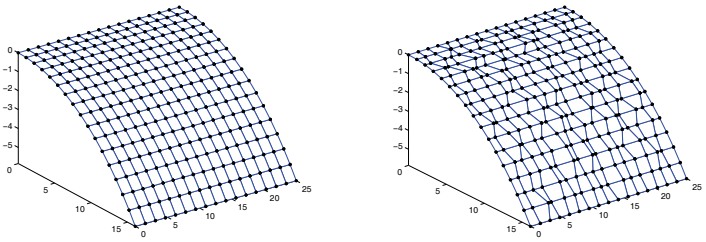

(a) (b)

Figure 7: The Scordelis-Lo roof: (a) typical regular mesh and (b) irregular mesh.

elements perform quite well in both types of mesh in comparison with the reference solution and other shell elements. The convergence of stress resultants obtained by uniform elements is also presented in Table 3.

Table 2: The Scordelis-Lo roof: displacements at point B, normalized by 0.3024

Model	Mesh			
	4×4	8×8	12×12	16×16
MISQ24 (regular mesh)	1.1912	1.0420	1.0154	1.0063
MISQ24 (irregular mesh)	1.1925	1.0422	1.0155	1.0066
SRI-4	0.964	0.984	–	0.999
RSDS-4	1.201	1.046	–	1.010
T029 (SAMCEF)	0.976	0.986	–	0.993
NMS-4F	1.047	1.005	–	0.997
QPH	0.940	0.980	–	1.010
DKQ-4	1.048	1.005	–	0.996
IBRA-4	1.047	1.005	–	0.997
URI-4	1.219	1.054	–	1.017

The numerical convergence is also plotted in Figure 8. As can be seen, the convergence rate of the present element for both types of mesh is nearly equivalent. It is also observed that the MISQ24's rate of convergence is slightly slower than that of the SRI-4 element. However, it is interesting to note that the MISQ24 element appears to converge monotonically to the reference solution even with a highly distorted mesh. Convergence rate of the present element in this problem indeed appear

Table 3: The Scordelis-Lo roof: Stress resultants (bending and membrane components)

Mesh	M_x^C	N_x^C	N_y^B
4×4	-2.162E3	-3.210E3	6.810E4
8×8	-2.081E3	-3.379E3	7.372E4
16×16	-2.062E3	-3.400E3	7.372E4

quite satisfactory.

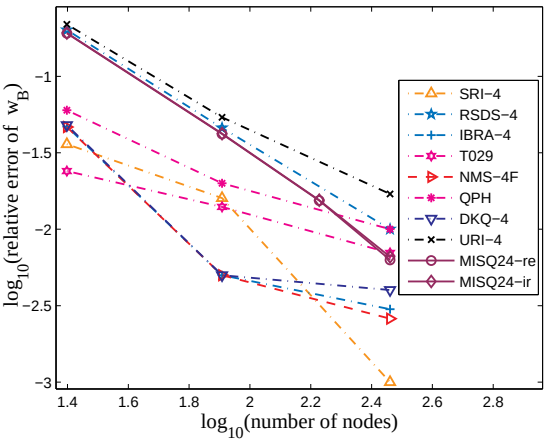

Figure 8: The Scordelis-Lo roof: Convergence behaviour

4.2 A pinched cylinder with end diaphragms

In this section, a pinched cylinder with end diaphragms is considered. This problem is regarded as one of the most severe tests for the performance of the element with the presence of both in-extensible bending and complex membrane states of stress. The cylinder is supported by rigid diaphragms at both ends and pinched with two opposite radial concentrated loads at the middle of the length. The geometrical and material properties of the cylinder are depicted in Figure 9.

Owing to symmetry, only one octant of cylinder is modelled with a mesh of uniform elements as well as distorted elements. Two typical meshes used in the analysis are shown in Figure 10.

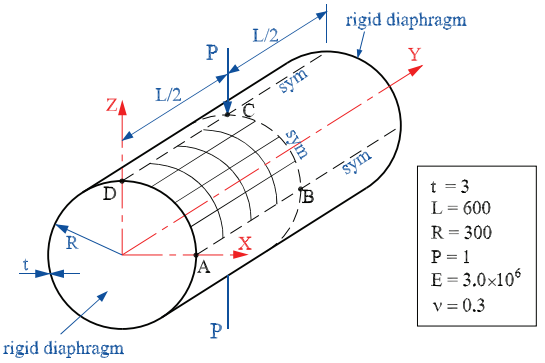

Figure 9: A pinched cylinder with end diaphragms: Geometry and material data

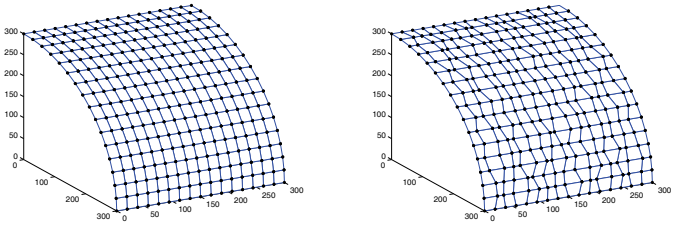

(a) (b)

Figure 10: A pinched cylinder with end diaphragms: (a) typical regular mesh and (b) irregular mesh.

The theoretical solution of the radial deflection at the loading point (point C) given by Ted Belytschko and Leviathan (1994) is 1.8248×10^{-5}. The present numerical results with meshes of 4×4, 8×8, 12×12 and 16×16 elements are compared versus other solutions from the literature using 4–node quadrilateral elements. All the numerical results, normalized with respect to the analytical value, are given in the Table 4. It is observed that the performance of the present element is in excellent agreement with the analytic solution for both types of mesh and are better than other shell elements considered in this study. The convergence of stress resultants at the loaded point obtained by uniform elements is also reported in Table 5.

The convergence behaviours of all cited elements are also plotted together in Figure 11. As it can be seen, the MISQ24 elements yield the most rapidly converging solutions to theoretical value. In the case of highly distorted elements, it is particularly interesting to point out that the present element faces no difficulties converging at the same rate as some of the most efficient contemporary four-node shell

Table 4: A pinched cylinder with end diaphragms: displacements at point C, normalized by: 1.8248×10^{-5}

Model	Mesh			
	4×4	8×8	12×12	16×16
MISQ24 (regular)	0.6416	0.9411	0.9921	1.0018
MISQ24 (irregular)	0.6478	0.9375	0.9915	1.0010
MIN4T	0.5040	0.8374	–	0.9619
XSHELL41	0.625	0.926	–	0.995
XSHELL42	0.625	0.918	–	0.992
SRI-4	0.373	0.747	–	0.935
RSDS-4	0.469	0.791	–	0.946
SHELL63(ANSYS)	0.6302	0.9371	–	1.0029
QC5D-SA	0.3759	0.7464	–	0.9300
QPH	0.370	0.740	–	0.930
IBRA-4	0.3704	0.7367	–	0.9343
DKQ-4	0.6357	0.9459	–	1.0160
MITC4	0.3699	0.7398	–	0.9300
Mixed	0.3989	0.7628	–	0.9349

Table 5: A pinched cylinder with end diaphragms: Stress resultants.

Mesh	M_x^C	N_x^C
8×8	1.381E-1	-6.501E-2
12×12	2.060E-1	-7.276E-2
16×16	2.464E-1	-7.362E-2

elements using uniform elements. The MISQ24's convergence rate is even slightly better than the SHELL63 element used in the commercial finite element software ANSYS for this problem.

4.3 A pinched hemispherical shell with an 18^0 *hole*

Figure 12 shows the hemispherical shell with an 18^0 hole subjected to concentrated diametrical loads of opposite signs every 90^0 in the equatorial plane. This problem is a very useful example to check the ability of the element to handle rigid body rotation about the normal to the shell surface and the inextensible bending modes. Shell elements with membrane locking cannot correctly solve this problem. Taking advantage of symmetry, a quadrant of the shell is modelled with uniform elements.

Table 6 shows numerical results for the radial displacement at the loading point (u_A)

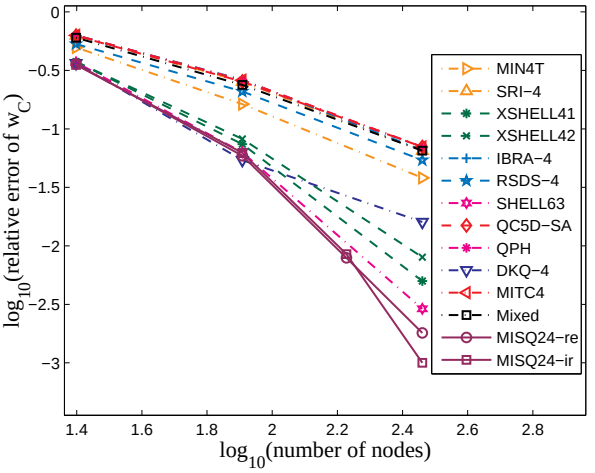

Figure 11: A pinched cylinder with end diaphragms: Convergence behaviour

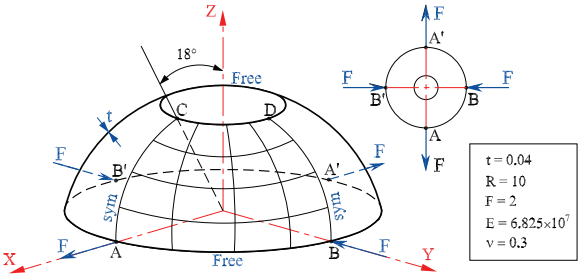

Figure 12: A pinched hemispherical shell with 18^0 hole: Geometry and material data

for different elements. The values are normalized with the theorical value of 0.094 reported by MacNeal and Harder (1985). All normalized radial displacements are also plotted in Figure 13 to assess the convergence behaviour of each element. It can be seen that the present element yields the most monotonic convergence towards the reference solution while some other elements do not. The plot also shows that the present element exhibits an excellent accuracy with a 16×16 mesh. No membrane locking is detected and the performance of the present element in this problem is remarkable.

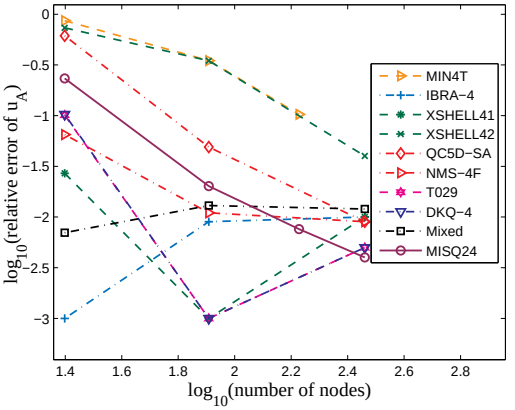

Figure 13: A pinched hemispherical shell with an 18^0 hole:Convergence behaviour

4.4 A hypar shell

A hyperbolic paraboloid shell or hypar shell (Figure 14) as proposed in Gruttmann and Wagner (2005) is studied. This problem is used to assess the performance of element in dealing with warped geometry and the effect of membrane locking. The geometry of the hypar shell is defined by the expression $z = \frac{xy}{8L}$. The shell is subjected to a uniform load p_z in the vertical direction with the following boundary conditions:
$w(-L/2,y) = w(L/2,y) = w(x,-L/2) = w(x,L/2) = 0;$
$u_A = u_B = 0;\ v_C = v_D = 0.$

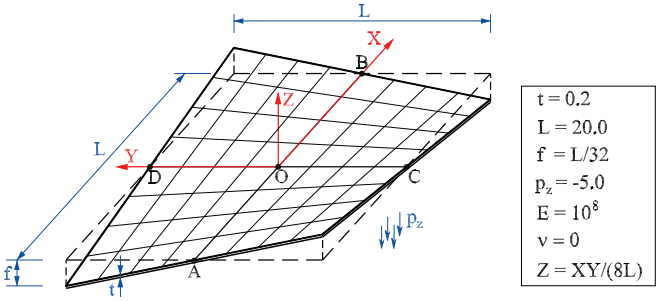

Figure 14: A hypa shell: Geometry and material data

The entire hypar shell is modelled and analysed with uniform elements. Table 7 presents the computed vertical displacement at the center point with different mod-

Table 6: A hemispherical shell with an 18^0 hole: displacements at point A, normalized by 0.0940

Model	Mesh			
	4×4	8×8	12×12	16×16
MISQ24 (regular)	0.7670	0.9798	0.9954	0.9960
MIN4T	0.136	0.651	0.897	–
IBRA-4	0.999	0.991		0.990
XSHELL41	1.027	1.001	–	0.990
XSHELL42	0.266	0.652	–	0.960
QC5D-SA	0.386	0.951	–	0.991
DKQ-4	0.897	0.999	–	0.995
NMS-4F	0.935	0.989	–	0.991
Mixed	0.993	0.987	–	0.988

els. The analytic solution for the central deflection ($w_0 = 4.6$) calculated by (Duddeck, 1962) is used for normalization. Numerical results indicate that the behaviour of the present element is in a close agreement with other reference solutions. It is observed that the present element does not show any sign of membrane locking even with coarse meshes. The element demonstrates an excellent performance where the displacement prediction error for the coarse mesh of 8×8 elements is about 0.35%.

Table 7: A hypar shell: central deflection w_0 for different elements, normalized by 4.6

Model	Mesh				
	4×4	8×8	16×16	32×32	64×64
MISQ24	0.978	0.994	0.998	0.999	1.000
DKQ-4	0.980	0.989	0.991	–	0.993
Sauer	0.980	0.991	0.996	–	1.000
GruWag	0.983	0.991	0.996	–	1.000

The displacements presented in Table 7 are also shown graphically in Figure 15 to assess the convergence with mesh refinement. As it can be seen from the plot, the present element does converge more quickly than elements cited here do for this problem.

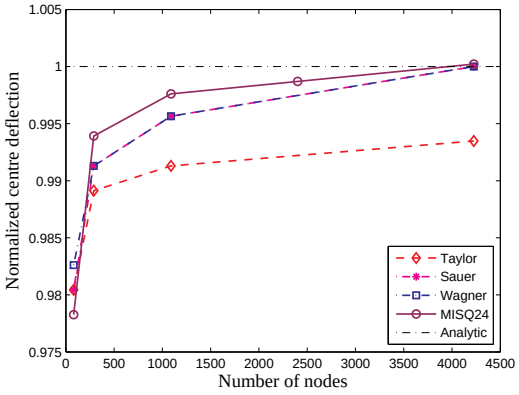

Figure 15: A hypar shell: normalized central deflections with mesh refinement

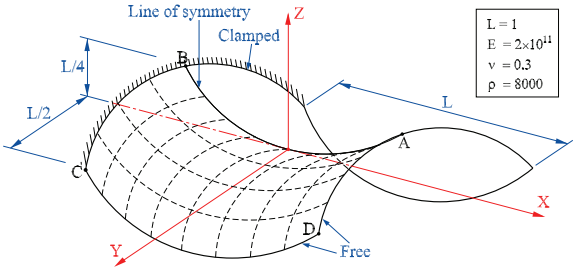

Figure 16: A partly clamped hypar shell: Geometry and material data

4.5 A partly clamped hyperbolic paraboloid shell

The problem considered in this section is that of a hyperbolic paraboloid shell, clamped along one side and free on three edges and loaded by self-weight (Figure 16). This is a pure bending dominated problem and known to be a very hard test for locking behaviour as suggested in References (Chapelle and Bathe, 1998; Bathe, Iosilevich, and Chapelle, 2000). The shell geometry is described by the equation: $z = x^2 - y^2; (x,y) \in \left[-\frac{L}{2}; \frac{L}{2}\right]$

One symmetric half of the shell, with uniform mesh patterns of $N \times N/2$ elements, is analyzed in the present work. To the author's knowledge, there is no analytic solution for this problem and the reference solution for displacement and strain energy obtained by Bathe, Iosilevich, and Chapelle (2000) with a refined mesh of high-order element MITC16, are used for comparison. Two thickness-to-length (t/L) ratios of 1/100 and 1/1000 are used to check locking behaviour of the present

element. The computed results are reported in Table 8 and Table 9 for displacements and strain energies, respectively.

Table 8: A partly clamped hypar shell: deflection at point A with mesh refinement.

Mesh	t/L=1/100		t/L=1/1000	
	MISQ24	MITC16	MISQ24	MITC16
8×4	9.9088E-5	–	7.1209E-3	–
16×8	9.4681E-5	–	6.7129E-3	–
32×16	9.3665E-5	–	6.4677E-3	–
48×24	9.3501E-5	9.3355E-5	6.4264E-3	6.3941E-3
64×32	9.3453E-5	–	6.4130E-3	–

Table 9: A partly clamped hypar shell: strain energy with mesh refinement

Mesh	t/L=1/100		t/L=1/1000	
	MISQ24	MITC16	MISQ24	MITC16
8×4	1.8028E-3	–	1.2512E-2	–
16×8	1.7073E-3	–	1.1633E-2	–
32×16	1.6858E-3	–	1.1155E-2	–
48×24	1.6822E-3	1.6790E-3	1.1077E-2	1.1013E-2
64×32	1.6812E-3	–	1.1055E-2	–

Figure 17 demonstrate the convergence of displacement and strain energy. It can be seen that the proposed element MISQ24 performs well, exhibiting insensitivity to the decrease in thickness.

4.6 A pre-twisted cantilever beam

A pre-twisted cantilever beam shown in Figure 18 is considered in this section. The cantilevered beam undergoes 90^0 of twist over its length. Two load cases are studied: a unit shear force P in the width direction and a unit shear force Q in the thickness direction. This example, proposed by MacNeal and Harder (1985), is an excellent test for assessing the element performance when the geometry configuration is warped. In the case of isotropic material, the theoretical deflections at the beam's tip are 0.00542 (in-plane shear P) and 0.001754 (out-of-plane shear Q), respectively, for the two load cases.

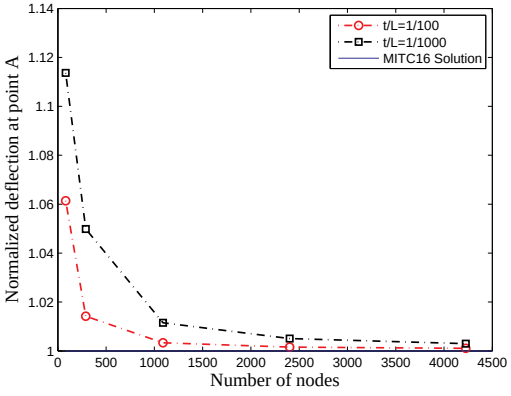

(a)

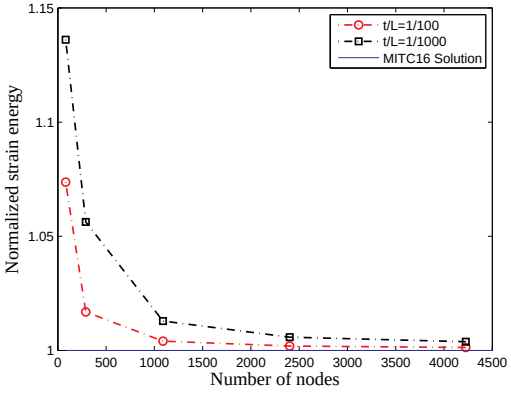

(b)

Figure 17: A partly clamped hypar shell: (a) Convergence of the deflection at point A and (b) convergence of the strain energy.

Table 10 presents the obtained results with mesh refinement together with other numerical solutions in the literature. It is observed that the MISQ24 element has no difficulties in dealing with warped geometries. Its performance is found to be better than that of some other elements cited here such as XSHELL42, RSDS-4 and MITC4 elements.

5 Conclusions

In this paper, an improved displacement-based 4-node flat shell element with drilling degrees of freedom has been developed and reported for geometrically linear analy-

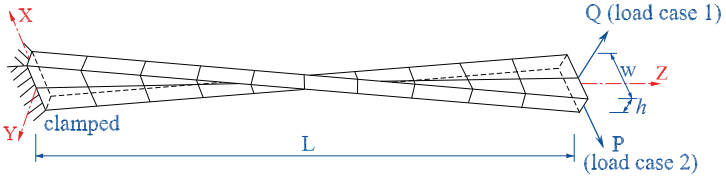

Figure 18: Pre-twisted cantilever beams: geometry and material data.

Table 10: Isotropic pre-twisted cantilever beam: tip displacements, normalized by 5.424×10^{-2} for in-plane displacements and by 1.754×10^{-2} for out-of-plane displacements.

Load case	Model	Mesh		
		2×6	4×12	4×24
In-plane	MISQ24	0.979	1.006	1.008
	DKQ-4	–	–	0.996
	XSHELL41	–	–	0.997
	XSHELL42	–	–	1.228
	RSDS-4	–	–	1.411
	MITC4	–	–	0.996
Out-of plane	MISQ24	0.811	0.928	1.015
	DKQ-4	–	–	0.998
	XSHELL41	–	–	0.999
	XSHELL42	–	–	1.473
	RSDS-4	–	–	1.361
	MITC4	–	–	0.974

sis of shell structures within the framework of the first-order shear deformation theory. The element is constructed basically by superimposing a membrane element with drilling degrees of freedom and an assumed strain plate-bending element. To enhance the basic behaviour of the element, the strain smoothing technique has been performed independently for membrane and bending strain parts. This technique allows integration, associated with the evaluation of bending and membrane parts of stiffness matrices, to be performed on the boundaries of the smoothing cells, which contributes to the high accuracy of the numerical solution. In some cases of mesh with certain level of distortion, the present element still shows better performance than that of other finite elements with uniform meshes. The smoothing operation also prevents numerical over-stiffening of the element, which helps

avoid membrane locking due to drilling DOFs.

Several numerical benchmark investigations are carried out to validate and demonstrate the efficiency and accuracy of the proposed element. The new flat shell element provides very excellent results to most of problems when compared with analytic solutions and referenced four-node shell elements in the literature. It is observed that the element is free of membrane and shear locking and could be a good candidate for general shell structural analysis in engineering practice where the range of thickness-to-length (t/L) ratio is usually from $1/10$ to $1/1000$.

Acknowledgement: The supports from the Faculty of Engineering and Surveying (FoES) and the Computational Engineering & Science Research Center (CESRC), USQ, Australia, are gratefully acknowledged. The authors would like to thank the referees for their helpful comments.

References

Allman, D. J. (1984): A compatible triangular element including vertex rotations for plane elasticity analysis. *Computers and Structures*, vol. 19, pp. 1–8.

Andelfinger, U.; Ramm, E. (1993): EAS-elements for two-dimensional, three-dimensional, plate and shell structures and their equivalence to HR-elements. *International Journal for Numerical Methods in Engineering*, vol. 36, pp. 1311–1337.

ANSYS (1998): *ANSYS User's Manual v5.5*, 1998.

Atluri, S. N. (1980): On some new general and complementary energy theorems for the rate problems in finite strain, classical elastoplasticity. *Journal of Structural Mechanics*, vol. 8, no. 1, pp. 61–92.

Atluri, S. N. (1984): Alternate stress and conjugate strain measures and mixed variational formulations involving rigid rotations, for computational analyses of finitely deformed plates and shells: Part-i: Theory. *Computers & Structures*, vol. 18, no. 1, pp. 93–116.

Atluri, S. N.; Cazzani, A. (1994): Rotations in computational solid mechanics. In *Archives for Computational Methods in Engineering, ICNME*, volume 2, pp. 49–138.

Bathe, K. J.; Dvorkin, E. N. (1985): A four node plate bending element based on Mindlin-Reissner plate theory and a mixed interpolation. *International Journal for Numerical Methods in Engineering*, vol. 21, pp. 367–383.

Bathe, K. J.; Iosilevich, A.; Chapelle, D. (2000): An evaluation of the MITC shell elements. *Computers and Structures*, vol. 75, pp. 1–30.

Belytschko, T.; Leviathan, I. (1994): Physical stabilization of the 4-node shell with one-point quadrature. *Computer Methods in Applied Mechanics and Engineering*, vol. 113, pp. 321–350.

Belytschko, T.; Lin, J. I.; Tsay, C.-S. (1984): Explicit algorithms for the nonlinear dynamics of shells. *Computer Methods in Applied Mechanics and Engineering*, vol. 42, pp. 225–251.

Belytschko, T.; Tsay, C.-S. (1983): A stabilization procedure for the quadrilateral plate element with one-point quadrature. *International Journal for Numerical Methods in Engineering*, vol. 19, pp. 405–419.

Belytschko, T.; Wong, B. L.; Stolarski, H. (1989): Assumed strain stabilization procedure for the 9-node Lagrange shell element. *International Journal for Numerical Methods in Engineering*, vol. 28, pp. 385–414.

Bischoff, M.; Bletzinger, K. (2001): Stabilized DSG plate and shell elements. In *Trends in Computational Structural Mechanics, CIMNE, Barcelona*, pp. 253–263.

Bischoff, M.; Ramm, E. (1997): Shear Deformable shell elements for large strains and rotations. *International Journal for Numerical Methods in Engineering*, vol. 40, pp. 4427–4449.

Cardoso, R. P. R.; Yoon, J. W.; Valente, R. A. F. (2006): A new approach to reduce membrane and transverse shear locking for one-point quadrature shell elements: linear formulation. *International Journal for Numerical Methods in Engineering*, vol. 66, no. 2, pp. 214–249.

Cardoso, R. P. R.; Yoon, J. W.; Valente, R. A. F. (2007): Enhanced one-point quadrature shell element for nonlinear applications. *International Journal for Numerical Methods in Engineering*, vol. 69, pp. 627–663.

Chapelle, D.; Bathe, K. J. (1998): Fundamental considerations for the finite element analysisof shell structures. *Computers and Structures*, vol. 66, pp. 19–36.

Chen, J.; Wu, C.; You, Y. (2001): A stabilized conforming nodal integration for Galerkin meshfree method. *International Journal for Numerical Methods in Engineering*, vol. 50, pp. 435–466.

Choi, C.-K.; Lee, P.-S. (1999): Defect-free 4-node flat shell element: NMS-4F element. *Structural Engineering and Mechanics*, vol. 8, pp. 207–231.

Choi, C.-K.; Lee, T.-Y. (2003): Efficient remedy for membrane locking of 4-node flat shell elements by non-conforming modes. *Computer Methods in Applied Mechanics and Engineering*, vol. 192, pp. 1961–1971.

Cook, R. D. (1994): Four-node 'flat' shell element: drilling degrees of freedom, membrane-bending coupling, warped geometry and behaviour. *Computers and Structures*, vol. 50, pp. 549–555.

Cui, X. Y.; Liu, G. R.; Li, G. Y.; Zhao, X.; Nguyen, T. T.; Sun, G. Y. (2008): A smoothed finite element method (sfem) for linear and geometrically nonlinear analysis of plates and shells. *CMES: Computer Modeling in Engineering & Sciences*, vol. 28, no. 2, pp. 109–125.

Duddeck, H. (1962): Die Biegetheorie der flachen hyperbolischen Paraboloidschale $z = \bar{c}xy$. *Archive of Applied Mechanics (Ingenieur Archiv)*, vol. 31, pp. 44–78.

Dvorkin, E. N.; Bathe, K. J. (1984): A continuum mechanics based four node shell element for general nonlinear analysis. *Engineering Computations*, vol. 1, pp. 77–88.

Eckstein, A.; Basar, Y. (2000): Ductile damage analysis of elasto-plastic shells at large inelastic strains. *International Journal for Numerical Methods in Engineering*, vol. 47, pp. 1663–1687.

Groenwold, A. A.; Slander, N. (1995): An efficient 4-node 24 DOF thick shell finite element with 5-point quadrature. *Engineering Computations*, vol. 12, pp. 723–747.

Gruttmann, F.; Wagner, W. (2005): A linear quadrilateral shell element with fast stiffness computation. *Computer Methods in Applied Mechanics and Engineering*, vol. 194, pp. 4279–4300.

Hughes, T. J. R.; Brezzi, F. (1989): On drilling degrees of freedom. *Computer Methods in Applied Mechanics and Engineering*, vol. 72, pp. 105–121.

Hughes, T. J. R.; Brezzi, F.; Masud, A.; Harari, I. (1989): Finite element with drilling degrees of freedom: Theory and numerical evaluations. In *Proceedings of the fifth international symposium on numerical methods in engineering*, pp. 3–17. Computational mechanics publications, Ashurst, U.K.

Hughes, T. J. R.; Cohen, M.; Haroun (1978): Reduced and selective integration techniques in finite element analysis of plates. *Nuclear Engineering Design*, vol. 46, pp. 203–222.

Hughes, T. J. R.; Liu, W. K. (1981): Nonlinear finite element analysis of shells: Part II. Two-dimensional shells. *Computer Methods in Applied Mechanics and Engineering*, vol. 27, pp. 167–182.

Ibrahimbegovic, A.; Frey, F. (1994): Stress resultant geometrically non-linear shell theory with drilling rotations. Part III: Linearized kinematics. *International Journal for Numerical Methods in Engineering*, vol. 37, pp. 3659–3683.

Ibrahimbegovic, A.; Taylor, R. L.; Wilson, E. L. (1990): A robust quadrilateral membrane finite element with drilling degrees of freedom. *International Journal for Numerical Methods in Engineering*, vol. 30, pp. 445–457.

Iura, M.; Atluri, S. N. (1992): Formulation of a membrane finite element with drilling degrees of freedom. *Computational Mechanics*, vol. 96, pp. 417–428.

Kim, K. D.; Lomboy, G. R.; Voyiadjis, G. Z. (2003): A 4-node assumed strain quasi-conforming shell element with 6 degrees of freedom. *International Journal for Numerical Methods in Engineering*, vol. 58, pp. 2177–2200.

Koschnick, F.; Bischoff, M.; Camprubi, N.; Bletzinger, K. (2005): The discrete strain gap method and membrane locking. *Computer Methods in Applied Mechanics and Engineering*, vol. 194, pp. 2444–2463.

Lee, P.-S.; Bathe, K.-J. (2004): Development of MITC isotropic triangular shell finite elements. *Computers & Structures*, vol. 82, no. 11-12, pp. 945–962.

Lee, S.; Pian, T. (1978): Improvement of plate and shell finite elements by mixed formulations. *AIAA Journal*, vol. 16, pp. 29–34.

Liu, G. R.; Dai, K. Y.; Nguyen, T. T. (2007): A smoothed finite element method for mechanics problems. *Computational Mechanics*, vol. 39, no. 6, pp. 859–877.

Liu, J.; Riggs, H. R.; Tessler, A. (2000): A four-node, shear-deformable shell element developed via explicit Kirchhoff constraints. *International Journal for Numerical Methods in Engineering*, vol. 49, pp. 1065–1086.

Liu, K. K.; Law, E. S.; Lam, D.; Belytschko, T. (1986): Resultant-stress degenerated-shell element. *Computer Methods in Applied Mechanics and Engineering*, vol. 55, pp. 259–300.

Long, C. S.; Geyer, S.; Groenwold, A. A. (2006): A numerical study of the effect of penalty parameters for membrane elements with independent rotation fields and penalized equilibrium. *Finite Element in Analysis and Design*, vol. 42, pp. 757–765.

MacNeal, R. H. (1978): A simple quadrilateral shell element. *Computer and Structures*, vol. 8, pp. 175–183.

MacNeal, R. H. (1982): Derivation of element stiffness matrices by assumed stain distribution. *Nuclear Engineering Design*, vol. 70, pp. 3–12.

MacNeal, R. H.; Harder, R. L. (1985): A proposed standard test problems to test finite element accuracy. *Finite Element in Analysis and Design*, vol. 1, pp. 3–20.

Nguyen-Van, H.; Mai-Duy, N.; Tran-Cong, T. (2007): A simple and accurate four-node quadrilateral element using stabilized nodal integration for laminated plates. *CMC: Computers, Materials & Continua*, vol. 6, no. 3, pp. 159–176.

Nguyen-Van, H.; Mai-Duy, N.; Tran-Cong, T. (2008a): A node-based element for analysis of planar piezoelectric structures. *CMES: Computer Modeling in Engineering & Sciences*, vol. 36, no. 1, pp. 65–96.

Nguyen-Van, H.; Mai-Duy, N.; Tran-Cong, T. (2008b): A smoothed four-node piezoelectric element for analysis of two-dimensional smart structures. *CMES: Computer Modeling in Engineering & Sciences*, vol. 23, no. 3, pp. 209–222.

Noor, A. K.; Peters, J. M. (1981): Mixed models and reduced/selective integration displacement models for nonlinear analysis of curved beams. *International Journal for Numerical Methods in Engineering*, vol. 17, pp. 615–631.

Pimpinelli, G. (2004): An assumed strain quadrilateral element with drilling degrees of freedom. *Finite Element in Analysis and Design*, vol. 41, pp. 267–283.

Samtech (2003): *Samcef User's Manual v10.1*, 2003.

Sauer, R. (1998): *Eine einheitliche Finite Element Formulierung fur Stabund Schalentragwerke mit endlichen Rotationen*. Bericht 4. Institut fur Baustatik, Universitat Karlsruhe (TH).

Simo, J. C.; Fox, F. D.; Rifai, M. S. (1989): On a stress resultant geometrically exact shell model. Part II: The linear theory; Computational aspects. *International Journal for Numerical Methods in Engineering*, vol. 73, pp. 53–92.

Simo, J. C.; Rifai, M. S. (1990): A class of mixed assumed strain methods and the method of incompatible models. *International Journal for Numerical Methods in Engineering*, vol. 29, pp. 1595–1638.

Stolarski, H.; Belytschko, T. (1983): Shear and membrane locking in curved C0 elements. *Computer Methods in Applied Mechanics and Engineering*, vol. 41, pp. 279–296.

Suetake, Y.; Iura, M.; Atluri, S. N. (2003): Variational formulation and symmetric tangent operator for shells with finite rotation field. *CMES: Computer Modeling in Engineering & Sciences*, vol. 4, no. 2, pp. 329–336.

Taylor, R. L. (1987): Finite element analysis of linear shell problems. In Whiteman, J.(Ed): *Proceeding of the Mathematics in Finite Element and Applications*. Academic Press, New York.

Yang, H. T. Y.; Saigal, S.; Masud, A.; Kapania, R. K. (2000): A survey of recent shell element. *International Journal for Numerical Methods in Engineering*, vol. 47, no. 1-3, pp. 101–127.

Zienkiewicz, O. C.; Taylor, R. L.; Too, J. M. (1971): Reduced integration technique in general analysis of plates and shells. *International Journal for Numerical Methods in Engineering*, vol. 3, pp. 275–290.